

Theory of the intermediate phase of $\text{SrCu}_2(\text{BO}_3)_2$ under pressure

C. Boos,^{1,2,*} S.P.G. Crone,³ I.A. Niesen,³ P. Corboz,³ K. P. Schmidt,^{1,†} and F. Mila^{2,‡}

¹*Institute for Theoretical Physics, FAU Erlangen-Nürnberg, Germany*

²*Institute of Physics, Ecole Polytechnique Fédérale de Lausanne (EPFL), CH 1015 Lausanne, Switzerland*

³*Institute for Theoretical Physics and Delta Institute for Theoretical Physics,*

University of Amsterdam, Science Park 904, 1098 XH Amsterdam, The Netherlands

(Dated: July 17, 2022)

Building on the NMR evidence that two different Cu sites are present in the intermediate phase of $\text{SrCu}_2(\text{BO}_3)_2$ under pressure, and on recent neutron scattering experiments, we investigate the nature of the intermediate phase in an orthorhombically distorted Shastry-Sutherland model. We show that a few percent difference between nearest-neighbor couplings is sufficient to destabilize the plaquette phase in favor of a quasi one-dimensional phase in which bonds around half the full plaquettes become stronger. This phase is adiabatically connected to the Haldane phase that is stabilized when next-nearest neighbor couplings take different values, and the excitations in this quasi one-dimensional phase are shown to agree qualitatively with neutron scattering results.

Almost two decades after the discovery of the first magnetization plateaus, the investigation of the layered material $\text{SrCu}_2(\text{BO}_3)_2$ under extreme conditions continues to attract a lot of attention and to reveal new fascinating properties. If there is by now ample evidence in favor of a sequence of magnetization plateaus at $1/8$, $2/15$, $1/6$, $1/4$, $1/3$, and $1/2$ (and possibly $2/5$) [1–10], the structure of some of these plateaus remains debated, and several groups are attempting to perform X-ray or neutron scattering in fields above 27 Tesla and at very low temperature to have direct information on the structure of the $1/8$ plateau. In parallel, the investigation of the phase diagram under pressure using various techniques ranging from NMR [11] to ESR [12] and neutron scattering [13] has revealed the presence of a phase transition at around 2.4 GPa to a new gapped phase that is the subject of the present paper.

$\text{SrCu}_2(\text{BO}_3)_2$ at ambient pressure is described to a very good accuracy by the Shastry-Sutherland model [14], also known as the orthogonal dimer model [15], defined by the Hamiltonian

$$H = J \sum_{\langle i,j \rangle} \vec{S}_i \cdot \vec{S}_j + J' \sum_{\langle\langle i,j \rangle\rangle} \vec{S}_i \cdot \vec{S}_j, \quad (1)$$

where J is the intra-dimer coupling and J' the inter-dimer coupling. In the limit $J' = 0$, the system consists of a set of decoupled dimers, and the exact ground state is a product of singlets on these dimers. Due to the frustrated nature of the inter-dimer coupling, this remains strictly true as long as J' is not too large. In the opposite limit $J = 0$, the system is a square lattice with nearest-neighbor antiferromagnetic couplings, and the ground state possesses long-range Néel order. In between, there is an intermediate phase that, after some debate [16–24], has been convincingly proven to be an

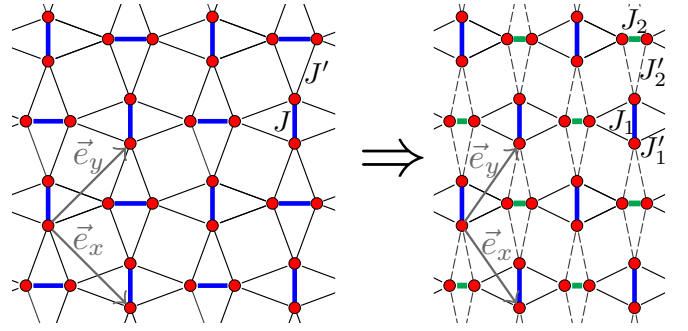


FIG. 1. The symmetric Shastry-Sutherland lattice, shown on the left, is orthorhombically distorted under pressure, which is illustrated on the right. The coupling strength of the compressed horizontal diagonals J_2 increases, whereas the diagonal couplings in the perpendicular direction J_1 remain unchanged. The nearest-neighbor couplings around the strengthened diagonals J'_2 decrease, the ones surrounding the weakened diagonals J'_1 increase. A unit cell contains a vertical and a horizontal dimer so that neighboring unit cells are connected by unit vectors \vec{e}_x and \vec{e}_y .

empty plaquette phase (EPP) and to exist in the range $0.675(2) < J'/J < 0.765(15)$ [25].

Since up to an overall energy scale the ratio J'/J is the only parameter of the Shastry-Sutherland model, applying hydrostatic pressure to change this ratio is a natural way to probe this phase diagram, and this has been first attempted in 2007 using NMR [11]. This experiment has indeed revealed the presence of a phase transition around 2.4 GPa, but in this intermediate phase, there are two types of Cu sites. This is incompatible with the EPP, which preserves a C_4 symmetry, and in which all Cu sites remain equivalent. The report of a weak orthorhombic distortion already at low pressure has led to the investigation of a model with two sets of intra-dimer couplings [26]. If the couplings are sufficiently different, another intermediate phase is realized. It is a one-dimensional phase related to a spin-one Haldane

* carolin.boos@fau.de

† kai.phillip.schmidt@fau.de

‡ frederic.mila@epfl.ch

chain. The main problem with this proposal is that the intra-dimer couplings need to be very different to stabilize this phase, making the proposal of Ref. [26] somewhat unrealistic.

More recently, neutron scattering experiments have confirmed the presence of a phase transition between 16 and 21.5 kbar and have provided evidence in favor of another transition at higher pressure, in agreement with the presence of an intermediate phase [13]. The structure factor is incompatible with the EPP, another indication that the intermediate phase is not that of the Shastry-Sutherland model, but it is compatible with a putative full-plaquette phase (FPP) in which bonds get stronger around plaquettes with diagonal couplings. These experiments have also revealed the presence of two excitation branches at very different energies, in sharp contrast with the dimer phase.

In this Letter, we show that all these proposals are actually consistent, and that a weak orthorhombic transition leads to an intermediate phase that is akin to both the FPP proposed in Ref. [13] and to the Haldane phase of Ref. [26]. This phase is of quasi one-dimensional character, leading to a natural explanation of the two modes revealed by neutron scattering.

Our results are obtained by two complementary methods, infinite projected entangled-pair states (iPEPS) and high-order series expansions (SE). An iPEPS is a variational tensor-network ansatz for two-dimensional ground states in the thermodynamic limit [28–30], where the accuracy is systematically controlled by the bond dimension D of the tensors. This approach has already been successfully applied in previous studies of the Shastry-Sutherland model, see e.g. Refs. [25, 31]. Details on the iPEPS approach, the optimization of the tensors (based on the full update scheme [32, 33]), and the procedure used to determine the phase boundaries are explained in the Supplemental Materials [27].

The SE for the ground-state energies of the EPP and FPP were performed by the Löwdin algorithm [34–36] while the energies of the elementary triplon excitations of the FPP have been determined using perturbative continuous unitary transformations (pCUTs) [37, 38]. In all cases we introduce a deformation parameter λ so that the unperturbed part $\lambda = 0$ corresponds to isolated (empty or filled) plaquettes and $\lambda = 1$ to the distorted Shastry-Sutherland model under study. The ground-state energy for the EPP (FPP) is calculated up to order 9 (8) in λ . The excitation energies of single triplons have been determined up to order 6 in both plaquette phases while for the specific one-dimensional case of the orthogonal-dimer chain ($J'_2 = 0$) order 8 has been reached. The derived orders are similar to other plaquette expansions [24, 39–41]. For the distorted Shastry-Sutherland model we increased the maximal perturbative order of the ground-state energies by two compared to Ref. 21. All series are extrapolated up to $\lambda = 1$ using Padé extrapolation [42]. In the following we use the variance of the different Padé extrapolants as uncertainty of the extrapolation. For de-

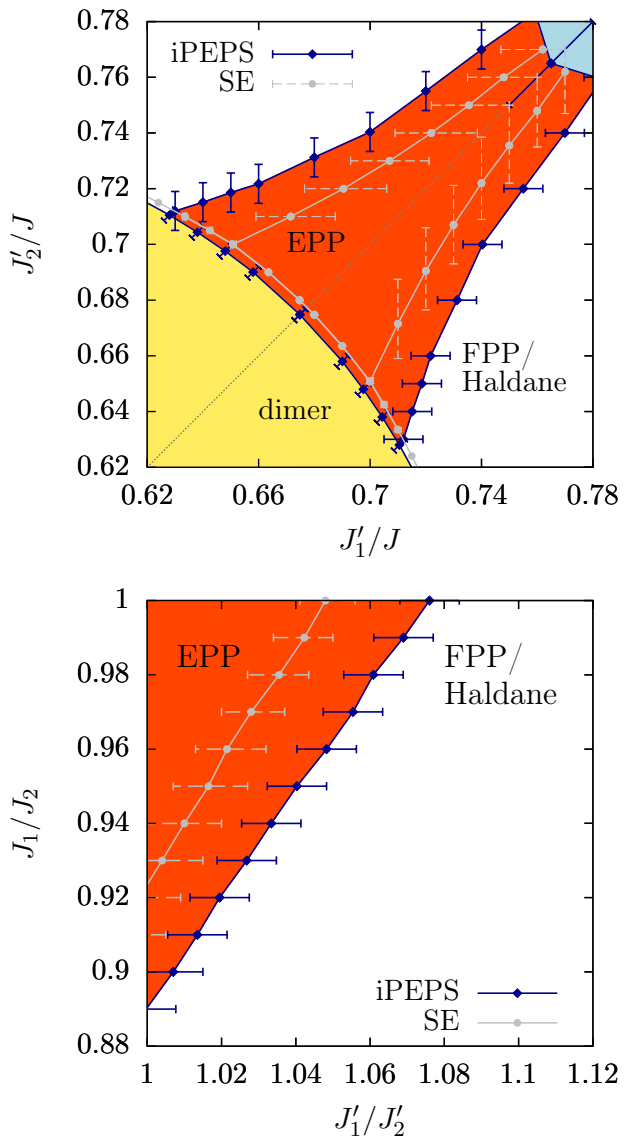


FIG. 2. Ground-state phase diagrams of distorted Shastry-Sutherland models by iPEPS and SE. The area of the dimer singlet phase is colored in yellow, the EPP in red, and the FPP/Haldane phase is shown in white. In the upper panel the diagonal couplings J_1 and J_2 are equal to J . In the lower panel a phase diagram for the completely asymmetric model with $J'_2/J_2 = 0.68$ is shown. For details see [27].

tails of the different SE as well as for the extrapolation we refer to the Supplemental Materials [27].

An orthorhombic distortion can be thought of as a compression of the lattice along a direction parallel to half the dimers and perpendicular to the other half (see Fig. 1). It leads to two sets of inequivalent J -bonds (J_1 and J_2), as assumed in Ref. [26], but also to two sets of inequivalent J' -bonds (J'_1 and J'_2 , see Fig. 1). Models with inequivalent J' -bonds have been introduced by Ref. 21 as starting points of SE, leading to a competition between the EPP and the FPP for the intermediate

phase of the Shastry-Sutherland model. These series expansion results have motivated the proposal of a FPP in Ref. 13. However, these phases are distinct (they do not break the same symmetries), and it is clear that only one of them can be realized for a given set of parameters.

To clarify this point, we have studied the model with inequivalent J' as well as J using SE and iPEPS. The resulting phase diagram of the distorted Shastry-Sutherland model with distinct nearest-neighbor interactions is shown in the upper panel of Fig. 2. The symmetric Shastry-Sutherland model is recovered along the diagonal of this phase diagram. As already demonstrated earlier the intermediate phase is the EPP [25], but it only takes a small distortion of the J' -couplings to drive the system into the FPP. So, if a small orthorhombic distortion takes place in the intermediate phase, it is possible to stabilize the FPP as suggested in Ref. [13].

Remarkably enough, the correlations in this phase look very similar to the correlations in the Haldane phase that is stabilized when intra-dimer couplings are assumed to have different values (see bottom right panel of Fig. 3 of Ref. [26]). So we have studied the general phase diagram of the Shastry-Sutherland model under an orthorhombic distortion, assuming that both inter- and intra-dimer couplings take different values. The results are exemplified in the lower panel of Fig. 2 for a cut at a fixed ratio of inter- to intra-dimer couplings $J'_2/J_2 = 0.68$. These results demonstrate that the FPP and the Haldane phase are adiabatically connected and constitute the same phase. Since this phase is consistent with NMR (it leads to two Cu sites) and with neutron scattering (it has the correlations typical of the FPP), it appears as a very strong candidate for the intermediate phase of $\text{SrCu}_2(\text{BO}_3)_2$.

To further demonstrate that the FPP and the Haldane phase are adiabatically connected we have computed the inter- and intra-dimer spin-spin correlations and the correlation lengths along a linear path in parameter space connecting the model with unequal inter-dimer couplings ($J'_2/J_2 = 0.66$, $J'_1/J'_2 = 1.1$, $J_1/J_2 = 1$) to the one with unequal intra-dimer couplings ($J'_2/J_2 = 0.55$, $J'_1/J'_2 = 1$, $J_1/J_2 = 0.5$). The iPEPS results ($D = 10$ full update simulations) in Fig. 3 show that all correlations change smoothly, i.e. that there is no sign of a quantum phase transition along this path. Interestingly, the ratio of the correlation lengths in x- and y-direction, ξ_x/ξ_y , remains almost constant along this path, revealing the anisotropic nature of this phase, that we will now call the FPP/Haldane phase, even in the limit of equal intra-dimer couplings ($J_1 = J_2$).

In the following we discuss the magnetic excitations of this quasi one-dimensional FPP/Haldane phase based on our SE results. Considering the limit $\lambda = 0$ of isolated filled plaquettes with $J_1 = J'_1$, it is apparent that there are two elementary triplon excitations with energy J'_1 , which can be characterized by the total spin $s_d = \{0, 1\}$ on the J_1 -dimers inside the plaquettes. In general, whenever the plaquettes are coupled, s_d is not a

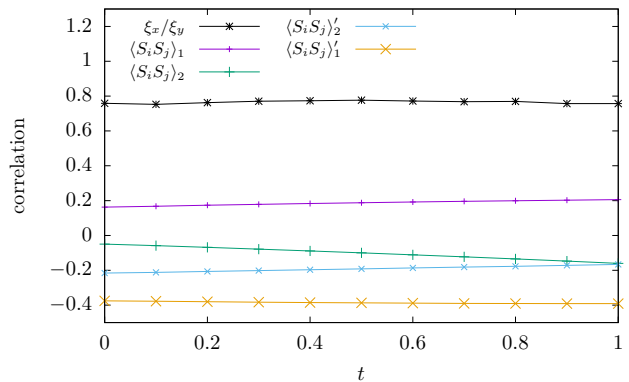


FIG. 3. Various correlations along a path connecting the model with only asymmetric diagonal couplings to the model with only asymmetric nearest-neighbor couplings. In particular it is $(J'_2/J_2, J'_1/J'_2, J_1/J_2) = (0.66 - 0.1t, 1.10 - 0.1t, 1 - 0.5t)$. The correlations with a prime $\langle \bullet \rangle'$ refer to nearest-neighbor bonds, the ones without a prime $\langle \bullet \rangle$ to the diagonal bonds. Additionally, the anisotropy in the correlation length ξ_x/ξ_y is shown.

conserved quantity and the two excitation branches are mixed. The effective one-triplon Hamiltonian in Fourier space is therefore given by the 2×2 -matrix $\Omega(\vec{k})$ resulting in two one-triplon bands $\omega_{\pm}(\vec{k})$.

We start the discussion with the one-dimensional orthogonal-dimer chain with distinct dimer couplings, i.e. the distorted Shastry-Sutherland model with $J'_2 = 0$ (chains are oriented horizontally in Fig. 1 that is along $\vec{e}_x + \vec{e}_y$). In that case, the two types of triplons are clearly characterized since the orthogonal-dimer chains host a local set of conserved quantities, the total spin s_d of the J_1 bonds. This total spin can be either $s_d = 0$ or $s_d = 1$ and the total Hilbert space decouples exactly in blocks with fixed quantum numbers s_d on each J_1 -dimer. The matrix $\Omega(\vec{k})$ is thus diagonal and the two one-triplon bands are associated with two different sectors of s_d . There is one triplon in the same sector as the FPP/Haldane ground state with all $s_d = 1$. This triplon can hop, and it acquires a finite dispersion with a gap Δ_H at $k_x + k_y = \pi$. The other triplon corresponds to converting one J_1 bond to $s_d = 0$. This singlet cannot move, and the band is flat. In the following we denote the gap of this flat mode by Δ_f . These one-triplon properties are best understood in the large J_2 limit, where the system reduces to an effective spin-one Heisenberg chain [26]. The dispersive mode is the one-magnon branch of the spin-1 chain, while the flat mode corresponds to the energy difference between the ground-state energies of the spin-one Heisenberg chain with open and periodic boundary conditions [27, 43]. The lowest-energy excitation can be either Δ_f or Δ_H depending on the specific choice of exchange couplings. In general, the Haldane gap Δ_H is lowest for J_2/J_1 large and the flat mode is lowest in the

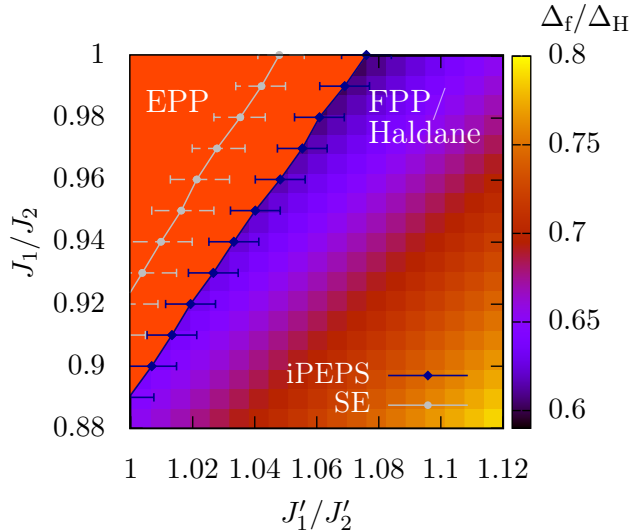


FIG. 4. Ratio Δ_f/Δ_H of the low-lying excitations in the FPP/Haldane phase at fixed $J'_2/J_2 = 0.68$ obtained from SE is displayed as a heat map together with the ground-state phase diagram from iPEPS and SE as in Fig. 2. For details see [27].

opposite case J_2/J_1 small [27].

Next we turn to the magnetic excitations of the FPP/Haldane phase for the two-dimensional distorted Shastry-Sutherland model. Even in the presence of the orthorhombic distortion, the system remains symmetric under the exchange of x - and y -direction. This translates into the properties $\Omega_{jj}(k_x, k_y) = \Omega_{jj}(k_y, k_x)$ with $j \in \{1, 2\}$ and $\Omega_{12}(k_x, k_y) = -\Omega_{12}(k_y, k_x)$ for the 2×2 matrix $\Omega(\vec{k})$. Consequently, the off-diagonal elements of $\Omega(\vec{k})$ vanish for $k_x = k_y$, i.e. along the direction of the orthogonal-dimer chains discussed above. In addition, $\Omega_{12}(\vec{k}) = 0$ at the discrete momenta $\vec{k} = (0, \pm\pi)$ and $\vec{k} = (\pm\pi, 0)$. For all other momenta the two one-triplet modes at $\lambda = 0$ mix due to the inter-plaquette couplings. Typically, the extrapolations of the SE work best for these momenta where $\Omega(\vec{k})$ is diagonal [27]. This is physically reasonable since the two one-triplet bands cannot mix and there are less decay processes into multi triplons. Note that we expect decay channels to be present in extended regions of the Brillouin zone whenever the bandwidth of the one-triplet modes is sufficiently large. This becomes most apparent around $\vec{k} = (0, 0)$ where the lower edge of the two-triplet continuum is approximately equal to twice the one-triplet gap. As a consequence, the higher-energy one-triplet mode decays quickly for finite inter-plaquette interactions [27]. We are therefore not able to provide reliable extrapolations of the two one-triplet bands $\omega_{\pm}(\vec{k})$ in the full Brillouin zone up to the experimentally relevant parameter regime.

Experimentally, the magnetic excitations have been in-

vestigated with inelastic neutron scattering only along the direction $\vec{k} = (k_x, 0)$ for specific values of k_x [13]. For each momentum two magnetic modes are observed which we identify with the modes $\omega_{\pm}(\vec{k})$. The minimal excitation energy for both modes is measured at $k_x = \pi$ where the ratio of the excitation energies is close to 0.5. Keeping in mind that $\Omega(\pi, 0)$ is diagonal, the two modes are directly equivalent to Δ_f and Δ_H . As already seen for the orthogonal-dimer chain, it depends on the choice of exchange couplings whether $\Delta_f/\Delta_H < 1$ or vice versa $\Delta_f/\Delta_H > 1$. Therefore, the experimental findings are consistent with both $\Delta_f/\Delta_H \approx 0.5$ and $\Delta_f/\Delta_H \approx 2$. In Fig. 4 we show the ratio Δ_f/Δ_H obtained from SE as a heat map together with the ground-state phase diagram for the same exchange couplings used in Fig. 2 (b). Interestingly, $\Delta_f/\Delta_H \approx 0.5$ holds close to the border to the EPP, the experimentally most realistic regime where the anisotropy of the exchange couplings is not too large. In this parameter regime the SE further predicts that the true gap is located along the diagonal close to $k_x = k_y = 0.25\pi$ (consistent with Ref. [24] for the symmetric Shastry-Sutherland model), and that it is given by the triplon branch associated with the Haldane mode [27]. As a consequence, the two triplon branches have to cross in the Brillouin zone.

Let us summarize our predictions for the intermediate phase of $\text{SrCu}_2(\text{BO}_3)_2$. First of all, it should be accompanied by an orthorhombic distortion that favors the formation of stronger J' -bonds around half the full plaquettes, and of weaker J -bonds inside these plaquettes. Second, the intermediate phase is consistent with both the Haldane phase of Ref. [26] and the FPP of Ref. [13], which are actually a unique phase that we have dubbed FPP/Haldane. Third, already small orthorhombic distortions of a few percent are sufficient to stabilize this phase. Fourth, two branches of triplon excitations are naturally present in this phase and their properties appear to be consistent with recent inelastic neutron scattering data for experimentally realistic exchange couplings. Overall, it would be highly desirable to perform further investigations of the magnetic excitations in the intermediate phase of $\text{SrCu}_2(\text{BO}_3)_2$ in order to pinpoint the exchange couplings either experimentally or with ab-initio calculations. It would be particularly interesting to perform inelastic neutron scattering along the $k_x = k_y$ line where the true one-triplet gap should be located according to our theory.

ACKNOWLEDGMENTS

This work was supported by the Swiss National Science Foundation (SNF). We acknowledge financial support by the German Science Foundation (DFG) through the Engineering of Advanced Materials Cluster of Excellence (EAM) at the Friedrich-Alexander University Erlangen-Nürnberg (FAU). This project has received funding from the European Research Council (ERC) under the Euro-

pean Union's Horizon 2020 research and innovation programme (grant agreement No 677061). The calculations have been performed using the facilities of the Erlangen Regional Computing Center (RRZE).

Supplementary Materials to "Theory of the intermediate phase of $\text{SrCu}_2(\text{BO}_3)_2$ under pressure".

C. Boos, S.P.G. Crone, I.A. Niesen, P. Corboz, K. P. Schmidt and F. Mila

The first part of these Supplementary Materials gives details on the iPEPS. In the second part the series expansion approaches for the ground-state energy and the excitations are discussed. This includes information on the convergence behavior of the various series. We then provide additional information on the asymmetric orthogonal-dimer chain. At last details on the excitation spectrum of the distorted Shastry-Sutherland model at some potentially experimental realistic parameters within the FPP/Haldane phase are given.

I. INFINITE PROJECTED ENTANGLED-PAIR STATES

An infinite projected entangled-pair state (iPEPS) [28–30] is an efficient tensor network variational ansatz tailored for systematically approximating ground states of two-dimensional lattice models in the thermodynamic limit. It can be seen as a natural extension of (infinite) matrix product states to two dimensions. On a square lattice, an iPEPS consists of a periodically repeated rectangular unit cell made up of five-legged tensors. Each tensor has a single physical leg representing the local Hilbert space of one or several lattice sites, and four auxiliary legs. The auxiliary legs connect to neighboring tensors such that the whole forms a square lattice network of tensors. The accuracy of the ansatz is systematically controlled by the dimension D of the auxiliary legs, called the bond dimension. The iPEPS ansatz used in the present work consists of a 2×2 unit cell, with one tensor per dimer (a similar ansatz was used in setup D in Ref. 44). In order to increase the efficiency of the simulations we implement a global $U(1)$ symmetry (a subgroup of the $SU(2)$ symmetry of the model) in the iPEPS tensors, see Refs. 45 and 46 for details.

Given a Hamiltonian \hat{H} , the goal of an iPEPS simulation is to find the optimal tensors that provide the best possible approximation to the ground state of \hat{H} . The simulation starts from either a randomly initialized or a previously converged state, which is then optimized using imaginary-time evolution by applying the operator $e^{-\beta\hat{H}}$ to the initial state for sufficiently large β . The evolution operator is split into a product of two-body operators by means of a Trotter-Suzuki decomposition. Application of the two-body operator to two neighboring tensors increases the dimension of the auxiliary bond connecting them, which then needs to be truncated back to the original dimension D . This can be done by using either the simple- [47] or full-update [32, 33] method. The former method truncates the updated bond by applying a singular-value decomposition to the tensors connected to the bond, and keeping only the D largest singular values. This approach is computationally inexpensive, but it does not provide the most optimal truncation. In contrast, the full update takes the whole wave function into account when truncating the updated bond, which is optimal, but computationally more demanding. In the present work we have run simple- and full-update simulations up to $D = 10$. We have also crosschecked our results for smaller D using variational optimization [48].

Once the optimized tensors have been obtained, expectation values can be calculated by contracting the infinite two-dimensional network formed by the iPEPS, its complex conjugate and the observable of interest. Since two-dimensional tensor networks cannot be exactly contracted in an efficient way, a controlled, approximate contraction method is required. In this work the contraction is done with the corner-transfer matrix (CTM) method [50, 54] adapted for a rectangular unit cell [51, 52]. The CTM introduces a new parameter, called the boundary dimension χ , which controls the accuracy of the contraction. We always choose χ to be large enough such that the error induced by χ is negligible compared to the error due to the finite D .

To determine the location of the phase boundaries between two phases, we first obtain two initial states biased towards both respective phases. The states are generated by evolving randomly initialized iPEPS in imaginary time with the simple-update method using a biased Hamiltonian. Next, using the biased initial states, we perform multiple simulations in the vicinity of the phase transition. Due to hysteresis, a state initialized in one phase will remain within this phase slightly beyond the transition point. The critical coupling is found by determining the point where the linearly interpolated energies of the two phases intersect. All the phase boundaries in Fig. 2 in the main text have been determined by this procedure, using $D = 10$ full-update simulations.

We have verified that finite D effects on the phase boundary are small by comparing the finite $D = 10$ results to the ones obtained by extrapolating the energies to the exact, infinite D limit, for the transition with fixed $J'_2/J_2 = 0.7$. The extrapolation is done based on the truncation error w which quantifies the degree of approximation in a state, and goes to zero in the exact limit (see Ref. 53 for details). Figure S1 shows the energies of the two plaquette states for different values of J'_1/J'_2 . For the unbiased Hamiltonian ($J'_1/J'_2 = 1$), we find that the empty plaquette phase (EPP) is clearly lower in energy than the full plaquette phase (FPP)/Haldane phase. When increasing J'_1/J'_2 , taking the extrapolated energies including their error bars into account, we find a transition value of $J'_1/J'_2 = 1.060(8)$. In comparison, the $D = 10$ result for the critical coupling is $J'_1/J'_2 = 1.058$, which is very close to the extrapolated

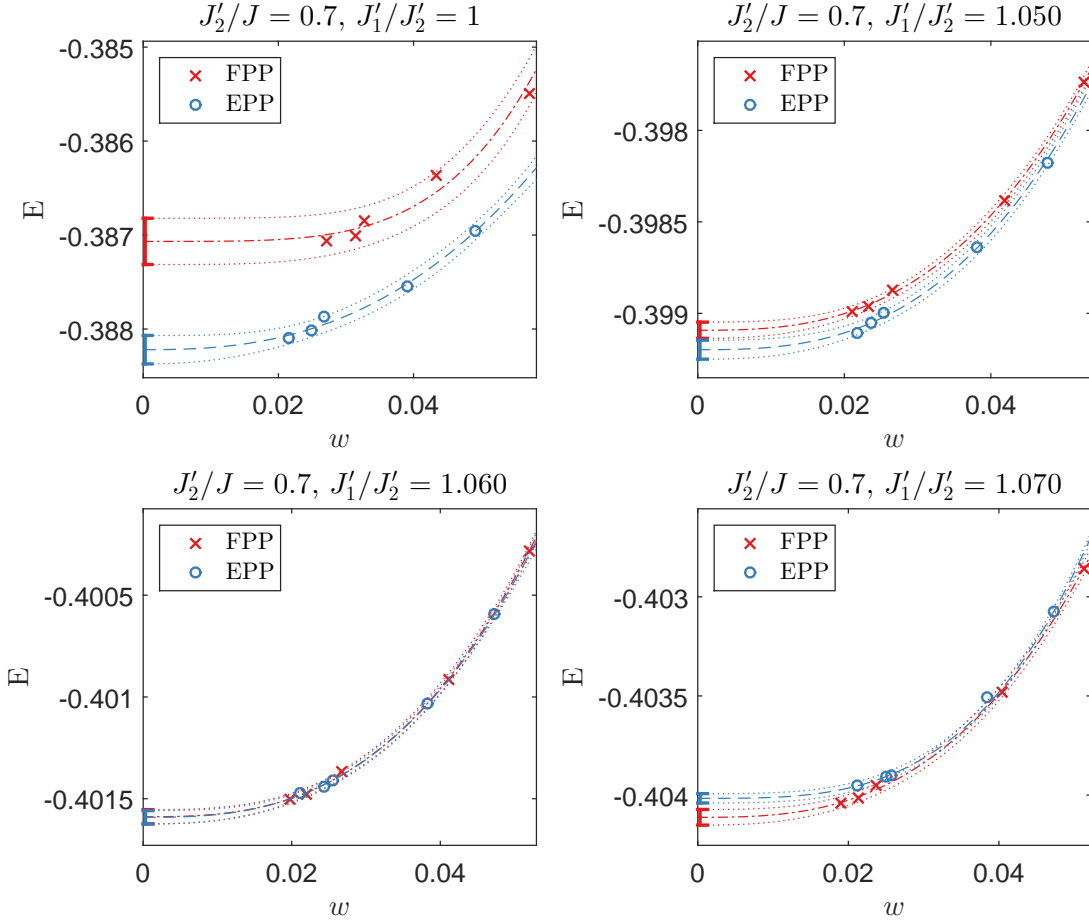


FIG. S1. Energy per site of the FPP/Haldane and EPP states as a function of the truncation error w obtained with iPEPS (using the full-update with bond dimensions ranging from $D = 6 \dots 10$), for different values of J'_1/J'_2 and fixed value of $J'_2/J'_2 = 0.7$. The extrapolations are obtained by a polynomial fit on the data, where the shown error is given by the 1σ confidence interval.

result and lies well within the extrapolation error bar. Thus, we conclude that the $D = 10$ result already provides a good accuracy of the phase boundary in the infinite D limit. We take the extrapolation error computed here as a representative error estimate of the phase boundary in Fig. 2 of the main text. The other error estimates in this figure between either the dimer or Néel phase and the EPP have been obtained from Ref. 44.

The simulations along the path in parameter space between the FPP and Haldane phase (Fig. 3 in the main text) have been obtained by $D = 10$ full-update simulations, starting from a state in the FPP. To exclude that the results are biased due to this choice of the initial state we have verified that the results at the end point of the path in the Haldane phase agree with the ones obtained when starting from randomly initialized tensors. We further note that the correlation lengths have been computed based on the largest and second largest eigenvalue of the row-to-row transfer matrix along both directions, as explained in Ref. [54].

II. SERIES EXPANSION METHODS

A. Ground-state energies

A subtle point about plaquette phases in the distorted Shastry-Sutherland model is given by the spatial location of the plaquette singlets. At first there is the obvious distinction between the location on either plaquettes containing or not containing an inner diagonal coupling, corresponding to the FPP or to the EPP, respectively. Besides, in each case, there is the choice of the subset of plaquettes on which the singlets are formed. In the case of the FPP, the singlets can either be on plaquettes formed by only J'_1 or J'_2 couplings. For identical dimer couplings $J_1 = J_2$ with the bias $J'_1 > J'_2$ the singlets are located on the J_1 plaquettes, whereas for $J'_2 > J'_1$ the J_2 plaquettes host the

singlets. Therefore, the FPP/Haldane phases shown in the upper panel of Fig. 2 of the main article actually represent two distinct phases which are separated by intermediate phases in this parameter range. For other parameters with $J_1 \neq J_2$ this is not necessarily the case, and in particular for $J_2 < J_1$ and $J'_1 > J'_2$ or vice versa, a direct phase transition between these two FPP/Haldane phases occurs. By contrast, the possibility to choose between two sets of empty plaquettes leads to a single EPP phase in Fig. 2 of the main article with a two-fold degenerate ground state.

For the ground-state energies per site ϵ_0 we apply perturbation theory after Löwdin [34–36] and perform linked-cluster expansions (LCEs). The series expansion (SE) about the FPP is performed from an unperturbed model of decoupled filled plaquettes at $\lambda = 0$. In the following we set the nearest-neighbor coupling of these plaquettes $J'_1 = 1$ and choose a diagonal coupling J_1 of intermediate strength $J_1^0 = 1/0.74$ at $\lambda = 0$. The diagonal coupling in the physical model at $\lambda = 1$ is then reached by an additional local perturbation on the diagonal bond. This approach for the FPP with such an initial value of J_1^0 turns out to be efficient to study a broad range of values, and is especially well converged in the area of interest. The Hamiltonian used for the SE of the FPP reads

$$\mathcal{H}^{\text{FPP}} = \sum_{\langle i,j \rangle}^{\text{bold}} \vec{S}_i \cdot \vec{S}_j + J_1^0 \sum_{\langle\langle i,j \rangle\rangle}^{\text{bold}} \vec{S}_i \cdot \vec{S}_j + \lambda_F J'_2 \sum_{\langle i,j \rangle}^{\text{thin}} \vec{S}_i \cdot \vec{S}_j + \lambda_F \Delta J_1 \sum_{\langle\langle i,j \rangle\rangle}^{\text{bold}} \vec{S}_i \cdot \vec{S}_j + \lambda_F J_2 \sum_{\langle\langle i,j \rangle\rangle}^{\text{thin}} \vec{S}_i \cdot \vec{S}_j, \quad (\text{S1})$$

where the sums can be understood with the lattice given in the left panel of Fig. S2. The diagonal couplings of the initial plaquettes are tuned to the physical value by $\Delta J_1 = J_1 - J_1^0$.

For the EPP the unperturbed model at $\lambda = 0$ is given by symmetric empty plaquettes. The inter-plaquette interactions are introduced perturbatively. Locally, the empty plaquettes in the distorted Shastry-Sutherland model exhibit different strengths on neighboring bonds of the plaquette, which is why an additional local interaction is introduced on two opposing bonds on the empty singlet plaquettes. The Hamiltonian used for the SE of the EPP is

$$\begin{aligned} \mathcal{H}^{\text{EPP}} = & \sum_{\substack{\langle i,j \rangle \\ \text{vertical} \\ \text{bold}}} \vec{S}_i \cdot \vec{S}_j + (1 + \lambda_E(J'_2 - 1)) \sum_{\substack{\langle i,j \rangle \\ \text{horizontal} \\ \text{thin}}} \vec{S}_i \cdot \vec{S}_j + \lambda_E \sum_{\substack{\langle i,j \rangle \\ \text{horizontal} \\ \text{bold}}} \vec{S}_i \cdot \vec{S}_j + \lambda_E J'_2 \sum_{\substack{\langle i,j \rangle \\ \text{vertical} \\ \text{thin}}} \vec{S}_i \cdot \vec{S}_j \\ & + \lambda_E J_1 \sum_{\langle\langle i,j \rangle\rangle}^{\text{bold}} \vec{S}_i \cdot \vec{S}_j + \lambda_E J_2 \sum_{\langle\langle i,j \rangle\rangle}^{\text{thin}} \vec{S}_i \cdot \vec{S}_j. \end{aligned} \quad (\text{S2})$$

Note, that the parameter spaces of the two deformed Hamiltonians linking the unperturbed product state of filled and empty plaquette singlets with the adiabatically connected states in the distorted Shastry-Sutherland model are not the same if $\lambda \neq 1$. We therefore refer to the expansion parameter in the expansion of the FPP with λ_F and to the expansion parameter in the expansion of the EPP with λ_E .

The perturbative description effectively takes place on a lattice of supersites, which are either given by one set of empty or of filled plaquettes. For all exchanges between these supersites transitions within a basis of 256 nearest-neighbor two-plaquette states occur. We exploit the linked-cluster theorem and perform a full graph expansion,

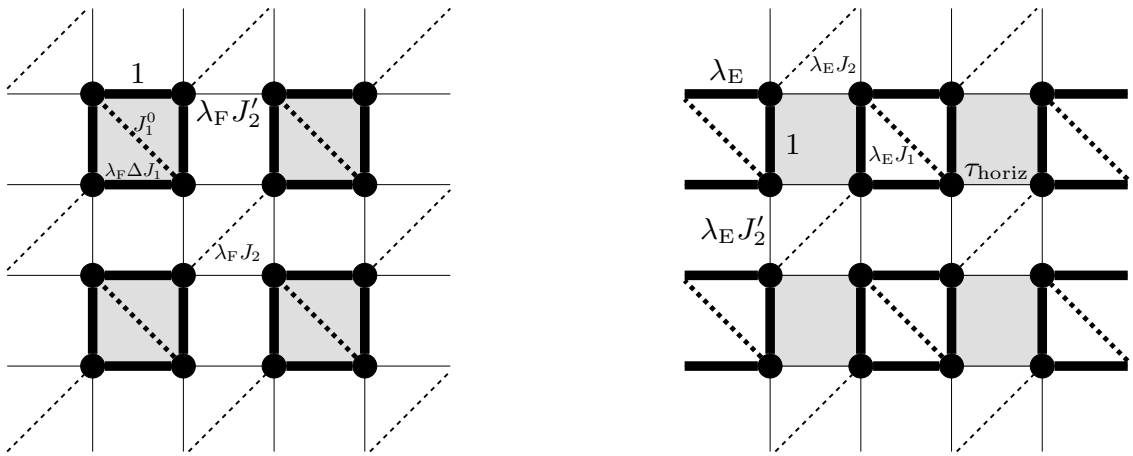


FIG. S2. Illustration of the models for the SE approaches. In the left panel the deformed Hamiltonian for the expansion about the full plaquette singlet state is indicated. The deformed Hamiltonian for the expansion of the empty plaquette state is shown in the right panel. The unperturbed plaquettes at $\lambda_F = 0$ or $\lambda_E = 0$ are shaded in gray. The exchange $\tau_{\text{horiz}} = 1 + \lambda_E(J'_2 - J'_1)$ introduces the asymmetry on the empty plaquettes hosting singlets.

where bonds of the same coupling need to be distinguished for different directions. For instance a trimer of three supersites has differing contributions for the direction $(2,0)^T$ and $(1,1)^T$ and hence needs to be calculated several times. This increases the number of required graphs for the ground-state energy ϵ_0 and one has to calculate the energy on 2849 graphs for the expansion in the FPP up to order eight in λ_F on a directed triangular lattice and 212 graphs on a directed square lattice for the expansion in the EPP in λ_E also in order eight. As a consequence the expansions cannot be pushed to similarly high orders as known for other models with smaller local Hilbert spaces of the supersites [24, 55, 56]. For the special case $J_1 = J_2$ or $J'_1 = J'_2$ order nine for the ground-state energy $\epsilon_0^{(E)}$ of the EPP is calculated. In that case, separate calculations on 244 graphs are required.

The polynomial series derived for the ground-state energies of both plaquette phases need to be analyzed carefully with respect to their convergence behavior. We apply Padé extrapolations which are given by rational functions. They are defined such that the Taylor expansion of the extrapolation equals the original series in the prevailing order [42]. The exponents of the numerator and denominator polynomials are referred to as $[l, m]$. An important issue for the usage of these extrapolations are spurious poles. If such a pole arises for an extrapolation in the parameter space of interest or in the close vicinity, the extrapolation has to be excluded from the physical analysis. The convergence behavior of the Padé extrapolations is analyzed by grouping them into families. All members of a family are characterized by the same difference $l - m$. If the extrapolations within one family show a convergent behavior, the member with the highest available order is taken as the best converged representant. The average about these representants from different families is considered as the most reliable result. In the following, we use the standard deviation of these extrapolants as a measure for the uncertainty. It is usually plotted as error bar. Another advantage of the Padé extrapolations as compared to the bare series is that they are better suited to control divergences for large values of λ . This is in particular true for all extrapolations with similar exponents in the numerator and denominator and the diagonal extrapolations with $l = m$ are expected to yield the most accurate results. In the following, we analyze the convergence behavior for the ground-state energies of the FPP/Haldane phase and EPP and state the detailed choices of Padé extrapolants. The main guideline is to average over extrapolations in the highest available order of every convergent family with similar exponents l and m .

For the pCUT expansion the dependencies of the energies from the parameters λ_F and λ_E at the coupling strengths $J'_2/J_2 = 0.68$, $J'_1/J'_2 = 1.01$ and $J_1/J_2 = 0.98$ are shown in Fig. S3 and Fig. S4, respectively. Displayed are the bare series in orders seven and eight, the Padé extrapolants $[3,5]$, $[5,3]$ and $[4,4]$ as well as the resultant mean value

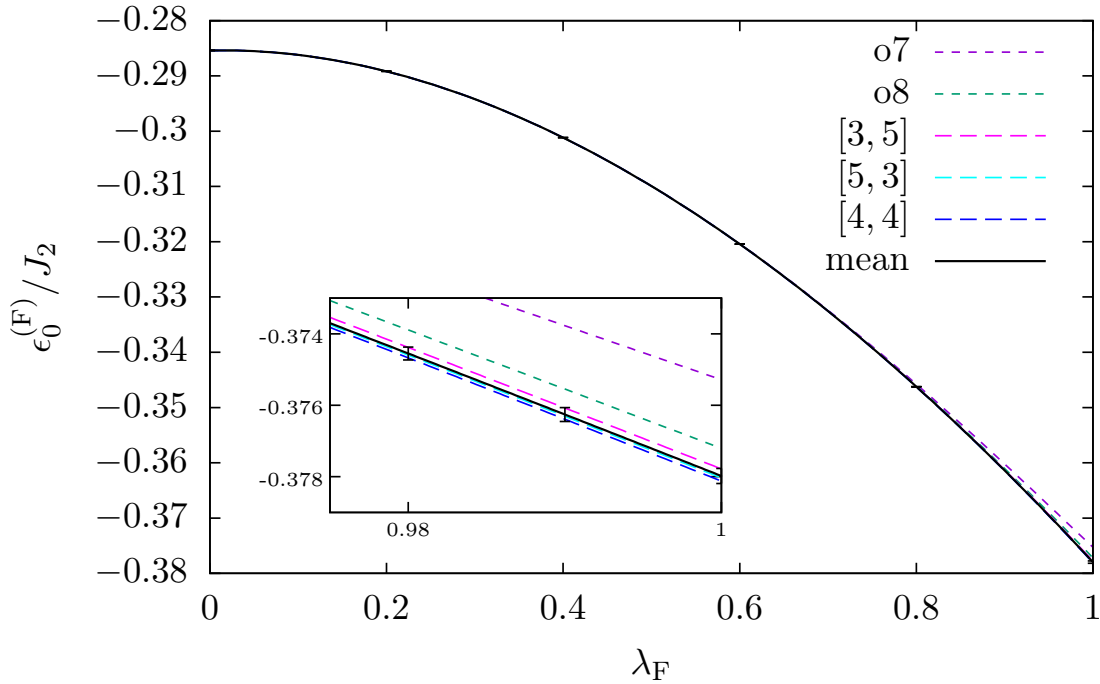


FIG. S3. Ground-state energies as bare series, Padé extrapolants and mean values of the expansion of the FPP/Haldane phase at $J'_2/J_2 = 0.68$, $J'_1/J'_2 = 1.01$ and $J_1/J_2 = 0.98$. The point $\lambda_F = 1$ belongs to the physically relevant distorted Shastry-Sutherland model.

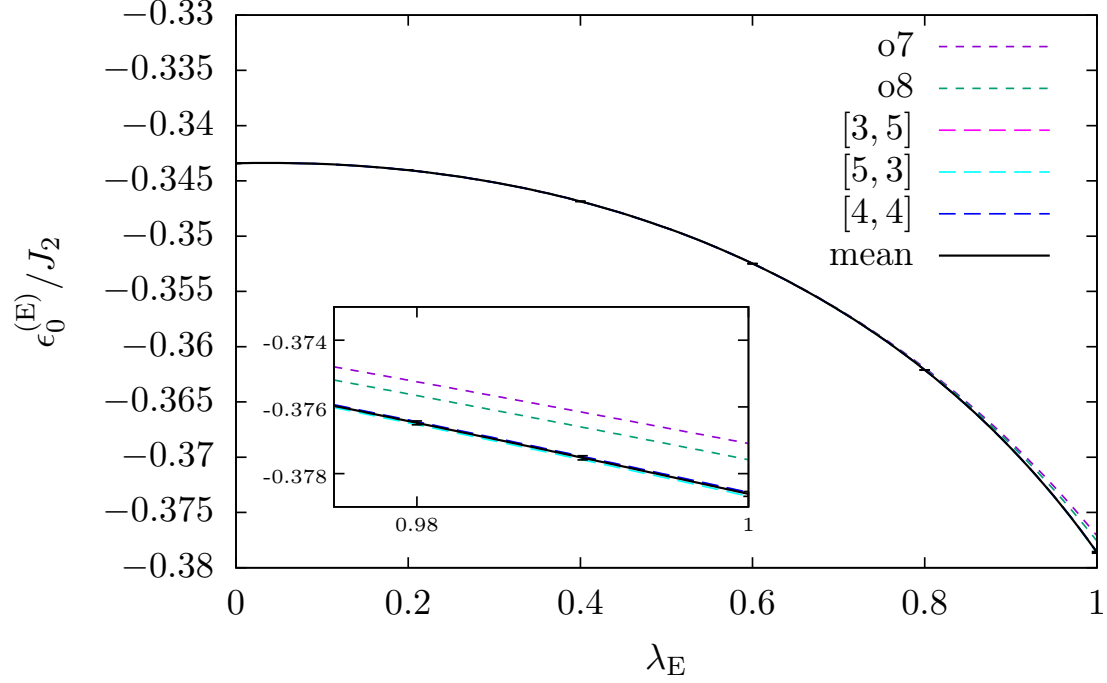


FIG. S4. Ground-state energies as bare series, Padé extrapolants and mean values of the expansion of the EPP at $J'_2/J_2 = 0.68$, $J'_1/J'_2 = 1.01$ and $J_1/J_2 = 0.98$. The point $\lambda_E = 1$ belongs to the physically relevant distorted Shastry-Sutherland model.

with the corresponding standard deviation taken from this set of extrapolants. The energies of both states decrease

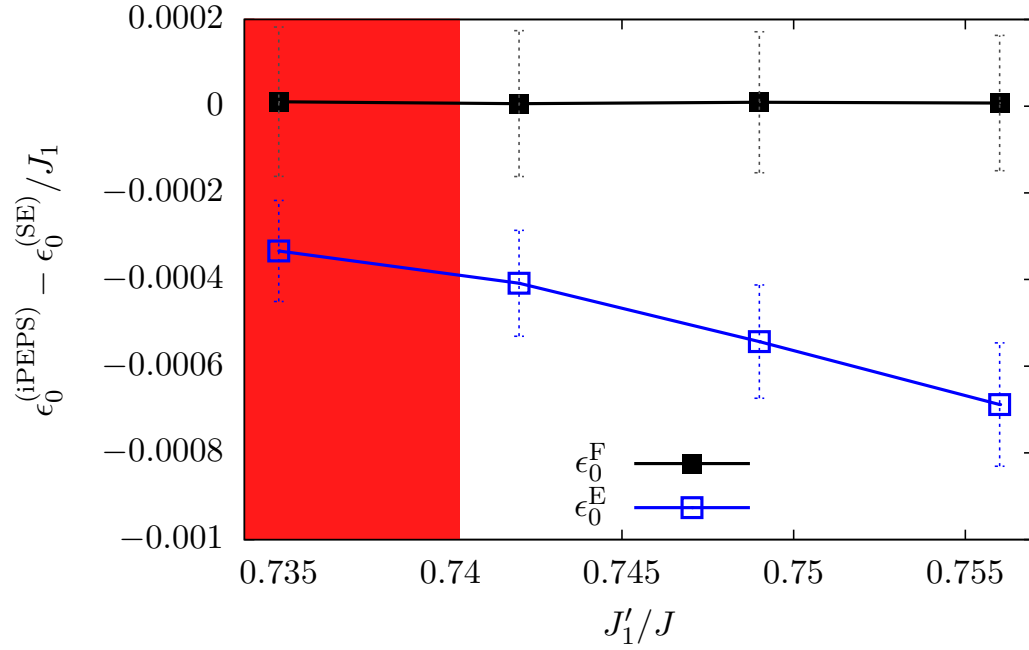


FIG. S5. Energy differences between ground-state energies from iPEPS and SE along the line $J'_2/J_2 = 0.7$ with $J_1/J_2 = 1$. The red background color indicates where the EPP is the ground state and no background color signals the FPP/Haldane phase as found by iPEPS.

with increasing expansion parameters due to quantum fluctuations. The difference between the unperturbed energy and the energy in the distorted Shastry-Sutherland model is more than twice as large for the FPP/Haldane phase in comparison to the EPP. This is due to the fact that the diagonal bond on a single plaquette increases the ground-state energy. Furthermore, the energy splitting between the bare series as well as the Padé extrapolants is larger for the FPP/Haldane phase at $\lambda_F = 1$ than for the EPP at these coupling values at $\lambda_E = 1$. The standard deviation of both phases becomes more similar in the parameter space where the FPP/Haldane phase is the ground state. This can be seen in Fig. S5, where the energy differences between the SE results to the iPEPS results is shown along the line $J'_2/J_2 = 0.7$ in the case $J_1/J_2 = 1$. For the EPP in this more symmetric case the series are reached up to order nine in λ_E and for the mean value the extrapolants [4,4], [4,5] and [5,4] are used. The FPP/Haldane phase energies of both approaches agree extremely well, whereas for the EPP the difference between iPEPS and SE energies is larger with a value of ≈ 0.0005 . This difference increases with the ratio J'_1/J_1 , since the asymmetry on the EPP supersites becomes stronger, which corresponds to a larger perturbation. The point in parameter space at $\lambda = 0$ is noticeably closer to the distorted Shastry-Sutherland model of interest or the FPP/Haldane phase than for the EPP. This is due to the fact that one of the strong diagonal couplings is mainly included in the unperturbed part of the FPP expansion. In this sense the perturbation for the EPP is larger, which might lead to an error on the EPP energies that is not reflected in the standard deviation of the Padé extrapolants, but would rather require higher order calculations to become evident.

For the analysis of the phase diagram in the upper panel of Fig. 2 in the main text we use the mean values of the energies as defined above in order eight for the FPP/Haldane phase and order nine for the EPP. In the phase diagram of the completely distorted Shastry-Sutherland model given in the lower panel of Fig. 2 in the main text both energies are taken as mean values of Padé extrapolants in order eight. The parameters where the standard deviations of the different expansions overlap are indicated as error bars.

B. Magnetic excitations of the FPP/Haldane phase

The magnetic excitations are calculated with SE using perturbative continuous unitary transformations (pCUTs) [37, 38], which allows to apply a LCE as well. For the pCUT the unperturbed problem is required to have an equidistant energy spectrum bounded from below. Considering an isolated plaquette, these conditions are fulfilled for a diagonal J_1 -bond $J_1^0 = 1$. It is then possible to rewrite the unperturbed part \mathcal{H}_0 of isolated plaquettes in Eq. (S1) for both cases as a counting operator \mathcal{Q} up to an additional constant E_0 . The perturbation $\lambda_F \mathcal{V}$ can be decomposed as a sum of operator \hat{T}_n with $n \in \{-4, \dots, +4\}$ with $[\hat{T}_n, \mathcal{Q}] = n\hat{T}_n$, i.e. the operators \hat{T}_n change the number of energy quanta by n . These energy quanta are called quasi-particles (QPs). The two deformed Hamiltonians can be written as

$$\mathcal{H} = E_0 + \mathcal{Q} + \lambda_F \sum_{n=-4}^4 \hat{T}_n \quad . \quad (\text{S3})$$

Within pCUTs, this type of Hamiltonian is unitarily mapped, order by order in λ_F , to an effective Hamiltonian \mathcal{H}_{eff} which conserves the number of QPs, i.e. $[\mathcal{H}_{\text{eff}}, \mathcal{Q}] = 0$. We note that this step can be done model-independent. The model-dependent part of pCUTs corresponds to a normal-ordering of the effective Hamiltonian in the QP sector of interest. This is done most efficiently via a full-graph decomposition using the linked-cluster theorem [57].

Here we focus on the one-QP sector with total spin one, which is the relevant sector for the comparison with inelastic neutron scattering (INS) measurements. Such magnetic triplet excitations are usually called triplons [58]. For $J_1^0 = 1$, there are two one-QP triplon modes which we have investigated with pCUTs. In practice, one determines all hopping amplitudes for these excitations up to some order in λ_F by calculating matrix elements of \mathcal{H}_{eff} between one-triplon states. The resulting one-QP hopping Hamiltonian can be further diagonalized by a Fourier transformation exploiting the translational symmetry of the lattice. Starting from the unperturbed plaquette with $J_1^0 = 1$, one gets the 2×2 matrix $\Omega(\vec{k})$ for each \vec{k} , which is easily diagonalized yielding two one-triplon dispersions $\omega_{\pm}(\vec{k})$. These one-triplon dispersions are determined up to order six in λ_F for the distorted Shastry-Sutherland model. For the simpler orthogonal-dimer chain with $J'_2 = 0$, we reach order eight in λ_F . Furthermore, in this one-dimensional set-up, the two one-triplon modes are protected by the local symmetry on the J_1 -bonds such that $\Omega(\vec{k})$ is directly diagonal. These decoupled modes are referred to as $\omega_{\text{H}}(\vec{k})$ and $\omega_{\text{f}}(\vec{k})$. In addition, we check whether the one-triplon modes have an infinite life-time by calculating the lower band edges $\omega_{\text{lowerbandedge}}^{ab}$ of the two-triplon continua of triplons $a, b \in \{\pm\}$. The lower band edge can be determined by

$$\omega_{\text{lowerbandedge}}^{ab}(\vec{k}) = \min_{\vec{q}} \left[\omega^a \left(\frac{\vec{k}}{2} + \vec{q} \right) + \omega^b \left(\frac{\vec{k}}{2} - \vec{q} \right) \right] \quad . \quad (\text{S4})$$

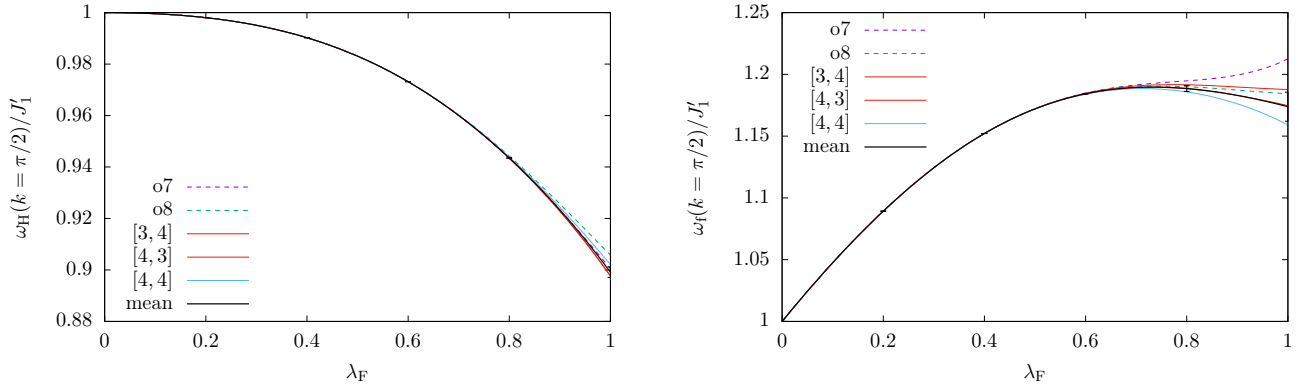


FIG. S6. Convergence of both one-triplon branches ω_H (left) and ω_f (right) at $J'_2 = 0, J_1 = 0.5$ and $J_2 = 1.2$ at $k = \pi/2$. Shown are the bare series in order seven and eight, several Padé approximants and their mean value with standard deviation as error bars.

If the one-triplon modes do not decay for a given wave vector \vec{k} , the calculated series of the various one-triplon modes can again be extrapolated by Padé approximation [42].

Next we illustrate the convergence behavior for some specific cases. For the distorted orthogonal-dimer chain the convergence behavior is illustrated for the parameters $J'_2 = 0, J_1 = 0.5$ and $J_2 = 1.2$ at $k = \pi/2$ ($k_x = \pi/2$ and $k_y = \pi/2$) in Fig. S6. At this set of parameters the series are well converged and a mean value of the Padé approximants [3,4], [4,3] and [4,4] is plausible. If one considers smaller values of k though, where the two-triplon continuum crosses with the dispersive one-triplon mode, the Padé approximants of this one-triplon excitation yield physical divergences corresponding to a finite decay of the mode into the two-triplon continuum. For the one-triplon dispersion and the two-triplon continuum shown in Fig. S7, we therefore take the mean value of the bare series in order seven and eight. The flat one-triplon mode is protected by symmetry and the mean value of the Padé approximants [3,4], [4,3] and [4,4] gives the most reliable result.

For the two-dimensional distorted Shastry-Sutherland model the convergence behavior is generically worse than for the orthogonal-dimer chain. This has several reasons. Firstly, we only reach the series up to order six. Secondly,

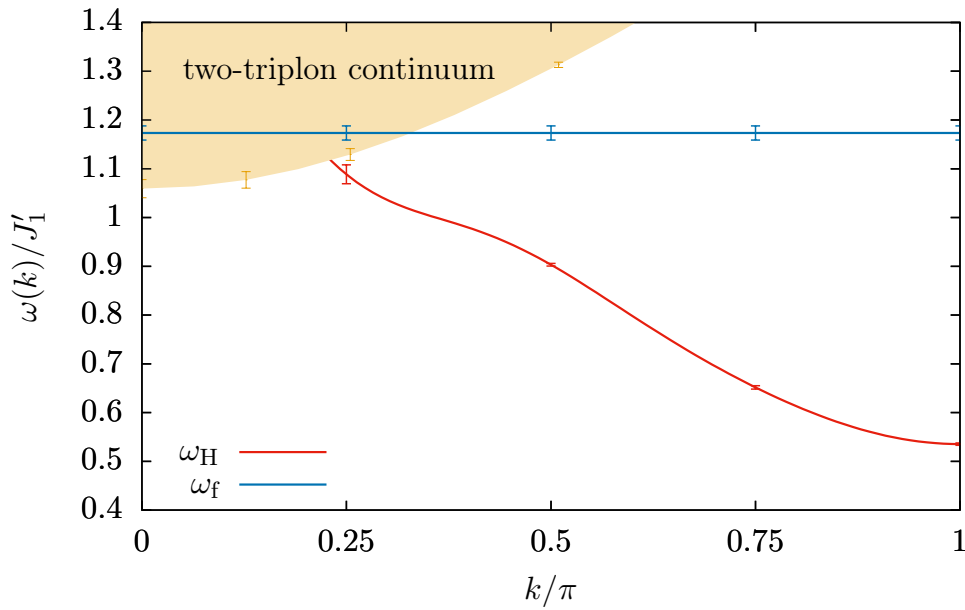


FIG. S7. Magnetic excitations of the asymmetric orthogonal-dimer chain in the FPP/Haldane phase at coupling values $J_1 = 0.5$ and $J_2 = 1.2$. This can be understood from the limit $J_2 \gg J_1, J'_1$. The excitation spectrum resembled the one of the Haldane phase on a spin-1 chain.

more perturbative exchange interactions have to be tuned to get from the unperturbed model to the two-dimensional model at $\lambda = 1$. At last, both triplon modes mix typically and therefore more quantum fluctuations contribute. For the specific momenta with $k_x = k_y$ as well as $(k_x = \pm\pi, k_y = 0)$ and $(k_x = 0, k_y = \pm\pi)$ the two triplon modes are protected, which is why we focus on these values. In Fig. 4 in the main text the ratios of the excitation energies at $(k_x = \pi, k_y = 0)$ are shown. For such ratios one can either choose to perform Padé extrapolations directly on the excitation energies and then calculate the ratio of these, or one can first derive the ratio and calculate the Padé extrapolation for this directly. It is not obvious which method is more valid. For Fig. 4 in the main text we first calculated the ratio of the bare series of both excitations and then extrapolated by the Padé approximants with exponents [2,3] and [3,2]. The background color shows the average of these two values. The Padé extrapolation with exponents [3,3] shows unphysical divergences in the chosen parameter space.

III. ASYMMETRIC ORTHOGONAL-DIMER CHAIN

In the limit $J'_2 = 0$ the distorted Shastry-Sutherland model reduces to decoupled orthogonal-dimer spin chains. This quasi one-dimensional model is very well suited to understand some of the main features also present in the distorted Shastry-Sutherland model. The phase diagram obtained with SE is shown in Fig. S8. It exhibits two phases both adiabatically connected to the case of completely decoupled filled plaquettes $J_2 = 0$: For weak diagonal couplings J_1 the ground state is determined by singlets on full plaquettes, where the total spin between both spins on both diagonals is one. This singlet phase is identical to the Haldane phase. At $J_1 = 2$ the ground state changes towards a state which has a total spin zero between the spins on the diagonals, and hence the spins connected by the J_1 coupling form a singlet. This is the exact dimer singlet phase.

In the following we give further information concerning the degenerate perturbation theory around the limit $J_2 \gg J_1, J'_1$ and $J_1 \gg J'_1$. It was previously applied for the asymmetric orthogonal-dimer chain up to second order [59] and for an extended Shastry-Sutherland model with distinct dimer couplings $J_1 \neq J_2$ in third-order perturbation theory [26]. The ground state of the unperturbed system is degenerate and consists of the manifold of states with a singlet on the J_2 bonds and isolated intermediate spins on the (vanishing) J_1 bonds. In third order in J'_1/J_2 the effective model is given by an effective frustrated Heisenberg ladder with rung couplings J_R , leg couplings J_L , and diagonal couplings between opposite sites of neighboring rungs J_\times . In particular it is $J_L = J_\times$. This effective model is identical for the Shastry-Sutherland model up to order three. Therefore, the FPP/Haldane phase in the two-dimensional model is of purely one-dimensional nature for large J_2 . In fourth-order perturbation theory additional effective four-spin interactions arise, and the distorted Shastry-Sutherland model is no longer described by a one-dimensional effective model. For the asymmetric orthogonal-dimer chain the effective Hamiltonian in order four is given by

$$\begin{aligned}
H_{\text{eff}}^{O(4)} = & \epsilon_0 N + J_R \sum_{\substack{i \\ \vdots \\ j}} \vec{S}_i \cdot \vec{S}_j + J_L \sum_{i-j} \vec{S}_i \cdot \vec{S}_j + J_\times \sum_{\substack{i \times j \\ 1 \times k}} \vec{S}_i \cdot \vec{S}_k + \vec{S}_j \cdot \vec{S}_l \\
& + J_K^R \sum_{\substack{i \quad j \\ \vdots \quad \vdots \\ 1 \quad k}} (\vec{S}_i \cdot \vec{S}_l)(\vec{S}_j \cdot \vec{S}_k) + J_K^L \sum_{\substack{i-j \\ 1-k}} (\vec{S}_i \cdot \vec{S}_j)(\vec{S}_l \cdot \vec{S}_k) + J_K^\times \sum_{\substack{i \times j \\ 1 \times k}} (\vec{S}_i \cdot \vec{S}_k)(\vec{S}_l \cdot \vec{S}_j),
\end{aligned} \tag{S5}$$

with the effective coupling parameters

$$\begin{aligned}
J_R &= J_1 - \frac{J'^2}{J_2} - \frac{1}{2} \frac{J'^3}{J_2^2} + \frac{5}{8} \frac{J'^4}{J_2^3}, \\
J_L &= \frac{1}{2} \frac{J'^2}{J_2} + \frac{3}{4} \frac{J'^3}{J_2^2} - \frac{5}{8} \frac{J'^4}{J_2^3}, \\
J_\times &= J_L, \\
J_K^R &= -\frac{1}{2} \frac{J'^4}{J_2^3}, \\
J_K^L &= \frac{J'^4}{J_2^3}, \\
J_K^\times &= J_K^L,
\end{aligned} \tag{S6}$$

and the constant

$$\epsilon_0 = -\frac{1}{4} \frac{J'^2}{J_2} - \frac{7}{8} \frac{J'^3}{J_2^2} + \frac{11}{8} \frac{J'^4}{J_2^3}. \quad (\text{S7})$$

For the further analysis the third-order model is particularly useful, since it has been studied before [43]. The total spin quantum number on every rung is conserved and in the limit $J_R \gg J_L$, or $J_2 \gg J'^2/J_1$, the system exhibits a ground state with singlets on every rung. At $J_R/J_L \approx 1.4$ a first-order phase transition towards a state, where all rungs are occupied by triplets, occurs. This state corresponds to a spin-1 chain and therefore is associated with the Haldane phase. In terms of the coupling constants of the asymmetric orthogonal-dimer chain the phase transition is at $J_1|_{\text{cr}} = 1.7 \frac{J'^2}{J_2} + 1.55 \frac{J'^3}{J_2^2} + 1.5 \frac{J'^4}{J_2^3}$, even though the fourth-order term is not exact due to the additional four-spin interactions. This phase transition is included as a red line in the phase diagram in Fig. S8 by the average of the bare second-, third-, and fourth-order results. From the same limit one can also extract statements concerning the magnetic excitation spectrum. The Haldane phase of the spin-1 chain exhibits a low-lying dispersive excitation. The minimum gives the Haldane gap $\Delta_H = 0.41$ at $k = \pi$ [60, 61]. This mode decays at small momenta, due to a continuum [60]. In terms of the frustrated ladder the energy gap is $\Delta_H = 0.41 J_L$. Another excitation is given by a rung singlet and is therefore completely localized. The excitation energy of this state is linked to the energy difference between a spin-1 chain with periodic and with open boundary conditions. It has been determined to be $1.21 J_L$ [43]. In terms of the frustrated ladder with an interaction on the bond of the flipped triplet we need to subtract the energy gained by the local singlet and find $\Delta_f = 1.21 J_L - J_R$. These relations together with the interaction constants of the effective model yield the parameters at which the ratio Δ_f/Δ_H between both excitation energies is equal to two

$$\left. \frac{J_1}{J'_1} \right|_{\Delta_f/\Delta_H=2} = 1.19 \frac{J'_1}{J_2} + 0.79 \left(\frac{J'_1}{J_2} \right)^2 - 0.87 \left(\frac{J'_1}{J_2} \right)^3. \quad (\text{S8})$$

The average of this result in orders two, three, and four is plotted as a dashed green line in Fig. S8. As outlined in the main body of the manuscript, the specific condition $\Delta_f/\Delta_H = 2$ is motivated from the INS data of $\text{SrCu}_2(\text{BO}_3)_2$ under pressure in the intermediate phase.

Similar information can also be gained by the SE from the limit with $J'_1, J_1 \gg J_2$, where at $\lambda = 0$ decoupled filled plaquettes are present. In this case the ground state of the unperturbed Hamiltonian is non-degenerate and the ground state energy follows directly from the SE, which we performed up to order eight in J_2/J'_1 and $\Delta J_1/J'_1$. We take the average value of the Padé extrapolations with the exponents [3,4], [4,3] and [4,4]. The phase diagram is represented in Fig. S8 by the plain yellow background color. In this area the dimer singlet phase is present. In the non-yellow area the FPP/Haldane phase occurs and the background color illustrates the ratio of the excitations at $k = \pi$, derived by SE from the limit $J'_1, J_1 \gg J_2$. For these ratios the Padé extrapolations of the ratios of excitation energies with exponents [3,4] and [4,3] are taken. In order to give an impression of the convergence behavior of the series we also plot two lines with explicit ratios $\Delta_f/\Delta_H = 2$ (blue) and $\Delta_f/\Delta_H = 1/2$ (cyan) including standard deviations of the extrapolations. For these standard deviations both extrapolation methods are employed. For the ratio $\Delta_f/\Delta_H = 1/2$ (cyan) the convergence behavior is very good and we see that it barely depends on J_2 . For the other case $\Delta_f/\Delta_H = 2$ at large inter-plaquette couplings $J_2 \lesssim 2$ the series are not very well converged, which is why the background is blank in this area. Nevertheless, the SEs from both limits can be seen to yield similar values at intermediate to large values of J_2 . At last a couple of phase transition points from the literature are included for comparison in the phase diagram in Fig. S8. In the symmetric case $J_1 = J_2$ our SE results agree very well with the value $J/J'|_{\text{cr}} = 1.22100$ by Koga *et al* [63]. Along the line $J_2 = 2J_1$ exact diagonalization by Richter *et al* revealed another transition point [59], which also matches our findings.

At last we give some additional information concerning the magnetic dispersion of the asymmetric-orthogonal dimer chain. Both low-energy excitations together with the continuum of two Haldane triplons are depicted for the parameters $J_1 = 0.5$ and $J_2 = 1.2$ in Fig. S7. The Haldane gap at $k = \pi$ is present and the corresponding dispersion increases with decreasing momentum. At values around $k \approx 0.45\pi$ nearly a saddle point can be observed, which becomes more pronounced for larger J_2 couplings and eventually transforms into a local maximum. For momenta close to $k = 0$ the Haldane mode decays into the continuum. All these three features are also known from the spin-1 Heisenberg chain [60] and this set of parameters is already somehow close to the Haldane limit with $J_2 \gg J'_1, J_1$ and $J_1 \gg J'_1$. The flat excitation at these parameters lies above the Haldane mode and also overlaps with the continuum. Nevertheless it does not decay since the total spins on the diagonals J_1 are conserved quantities. The overall structure of the excitation spectrum depends qualitatively on the coupling values. For instance for $J_1 = 1.5$ the flat mode is lower in energy than the Haldane gap, which can be seen in Fig. S8.

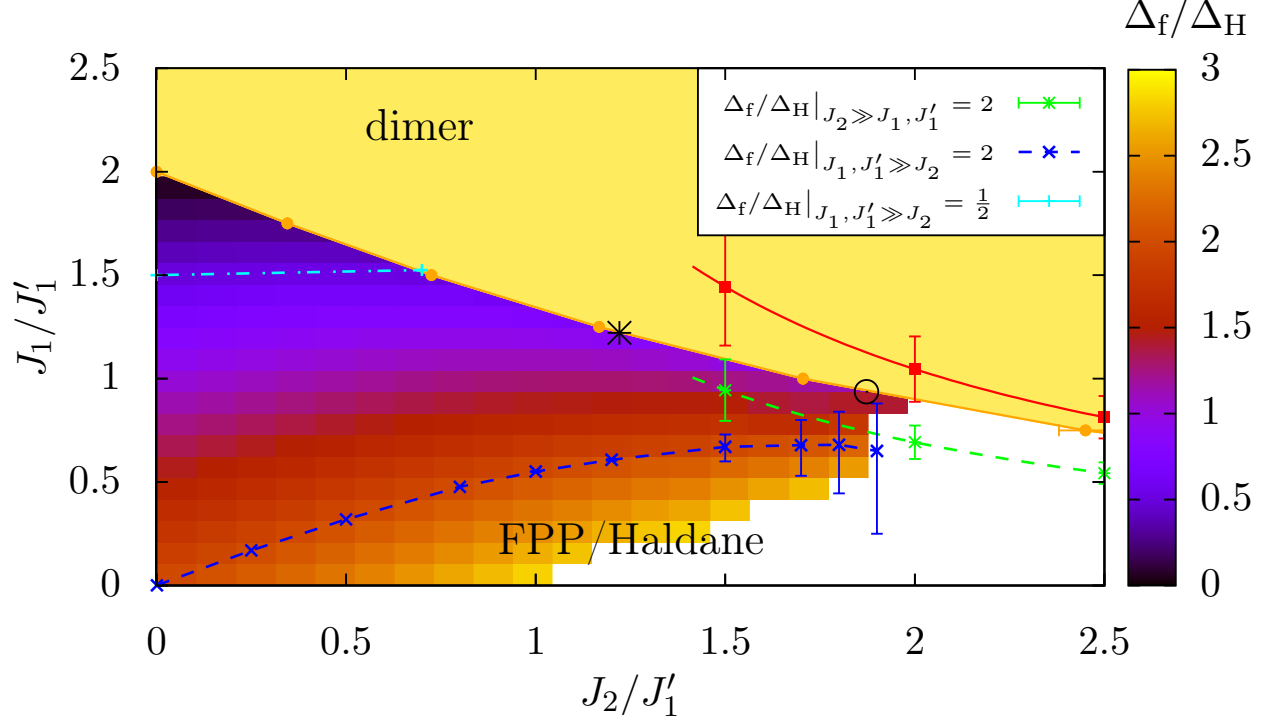


FIG. S8. The phase diagram of the orthogonal-dimer chain with distinct dimer couplings J_1 and J_2 . The background color shows results derived by SEs around the limit $J_1', J_1 \gg J_2$. The yellow area represents where the dimer singlet phase is present. Everywhere else the system is in the FPP/Haldane phase, and we show the ratio of the excitations at $k = \pi$ as the background color. Additionally, the ratios $\Delta_f/\Delta_H = 2$ and $\Delta_f/\Delta_H = 1/2$ are plotted as dashed lines. The phase transition is illustrated as a red line. The ratio $\Delta_f/\Delta_H = 2$ is given as a dashed green line. For more details see the text. For comparison two phase transition points from previous works are shown: i) as a black empty circle from [62] and ii) as a black star from [63].

IV. MAGNETIC EXCITATIONS OF THE DISTORTED SHASTRY-SUTHERLAND MODEL IN THE FPP/HALDANE PHASE

In addition to the findings on the magnetic excitations of the distorted Shastry-Sutherland model in the FPP/Haldane phase presented in the main body of the manuscript, here we give our results along the momentum direction of the orthogonal-dimer chains $k_x = k_y$. This direction is favorable with the SE because both triplon modes do not mix, which leads to a better convergence behavior of the excitation energies. The magnetic excitation spectrum of the FPP/Haldane phase for the coupling constants $J_1 = 1.33$, $J_2 = 1.4$ and $J_2' = 0.95$ along the line $k_x = k_y$ is given in Fig. S9. For these coupling constants one finds $\Delta_f/\Delta_H \approx 2$ (see Fig.4 of the main body of the manuscript) which is in agreement with the INS data of $\text{SrCu}_2(\text{BO}_3)_2$ under pressure in the intermediate phase. In Fig. S9 we show the two triplon modes ω_H and ω_f as well as the two-triplon continuum. For all quantities the Padé extrapolants with the exponents [2,3], [3,2] and [3,3] are considered. We then choose the subset of extrapolants without spurious poles. Note, that for small momenta k_x only one of the extrapolants for ω_H gives a valid result. The overall lowest excitation energy is given by the Haldane mode ω_H , which yields the energy $(0.178 \pm 0.002)J_1'$ close to $(k_x, k_y) = (0.25\pi, 0.25\pi)$. We expect this to be the true gap of the system. Even though we cannot make precise statements in the full Brillouin zone, the tendencies for increasing perturbations λ suggest that no excitation energy at other k -points gets lower in energy. At $(k_x, k_y) = (\pi, 0)$, where the minimum was measured by INS, the excitation energy is $(0.51 \pm 0.01)J_1'$. Interestingly, the two excitations at $(k_x, k_y) = (0.25\pi, 0.25\pi)$ and $(k_x, k_y) = (\pi, 0)$ are not of the same type, i.e. the true gap arises from the Haldane mode ω_H , whereas the minimum in the excitation energies at $(k_x, k_y) = (\pi, 0)$ stems from the mode that is connected to the flat mode of the orthogonal-dimer chain ω_f . For momentum values $k_x \gtrsim 0.4\pi$ as well as around $k_x = 0$ the lower mode ω_H decays into the two-triplon continuum. At small momenta this continuum consists of two Haldane modes ω_H , which is why the other mode ω_f does not decay here. For large momentum values the relevant continuum is formed by one triplon of each type and in principle both

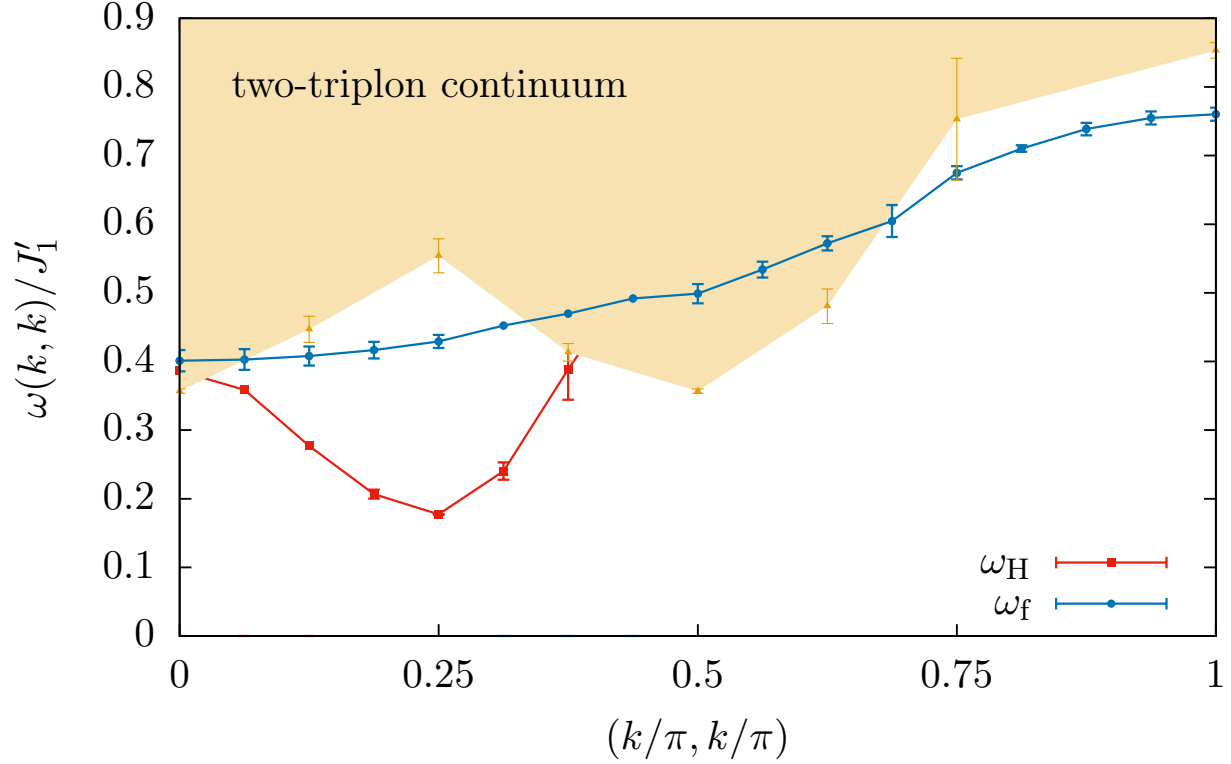


FIG. S9. Magnetic excitations of the distorted Shastry-Sutherland model at coupling values $J_1 = 1.33$, $J_2 = 1.4$ and $J'_2 = 0.95$ along the line in momentum space where $k_x = k_y \equiv k$. Single-triplet branches ω_H (ω_f) are shown in red (blue). Orange triangles corresponds to the lower band edge of the two-triplet continuum. Error bars indicate in all cases the uncertainty of the Padé extrapolation.

modes could decay. For the specific choice of coupling constants this does not occur for ω_f along $k_x = k_y$. Finally, the continuum set up by two modes ω_f is higher in energy.

Along the direction in momentum space where $k_y = 0$ the quality of convergence at intermediate values of k_x is worse than for $k_x = k_y$. This is related to the fact that both triplon modes for momenta $0 < k_x < \pi$ and $k_y = 0$ mix and therefore more quantum fluctuations are present, which have to be captured by the SE. Another reason for the poor convergence is the interference with continua. At momentum $k_x = k_y = 0$ where the continuum is below the one-triplet energy ω_H , only one Padé extrapolation does not show spurious poles.

-
- [1] H. Kageyama, K. Yoshimura, R. Stern, N. V. Mushnikov, K. Onizuka, M. Kato, K. Kosuge, C. P. Slichter, T. Goto, and Y. Ueda, *Phys. Rev. Lett.* **82**, 3168 (1999).
 - [2] K. Onizuka, H. Kageyama, Y. Narumi, K. Kindo, Y. Ueda, and T. Goto, *J. Phys. Soc. Jpn.* **69**, 1016 (2000).
 - [3] K. Kodama, M. Takigawa, M. Horvatić, C. Berthier, H. Kageyama, Y. Ueda, S. Miyahara, F. Becca, and F. Mila, *Science* **298**, 395 (2002).
 - [4] M. Takigawa, K. Kodama, M. Horvatić, C. Berthier, H. Kageyama, Y. Ueda, S. Miyahara, F. Becca, and F. Mila, *Physica B: Condensed Matter* **346–347**, 27 (2004).
 - [5] F. Levy, I. Sheikin, C. Berthier, M. Horvatić, M. Takigawa, H. Kageyama, T. Waki, and Y. Ueda, *EPL* **81**, 67004 (2008).
 - [6] S. E. Sebastian, N. Harrison, P. Sengupta, C. D. Batista, S. Francoual, E. Palm, T. Murphy, N. Marcano, H. A. Dabkowska, and B. D. Gaulin, *PNAS* **105**, 20157 (2008).
 - [7] M. Jaime, R. Daou, S. A. Crooker, F. Weickert, A. Uchida, A. E. Feiguin, C. D. Batista, H. A. Dabkowska, and B. D. Gaulin, *PNAS* (2012), 10.1073/pnas.1200743109.
 - [8] M. Takigawa, M. Horvatić, T. Waki, S. Krämer, C. Berthier, F. Lévy-Bertrand, I. Sheikin, H. Kageyama, Y. Ueda, and F. Mila, *Phys. Rev. Lett.* **110**, 067210 (2013).
 - [9] Y. H. Matsuda, N. Abe, S. Takeyama, H. Kageyama, P. Corboz, A. Honecker, S. R. Manmana, G. R. Foltin, K. P. Schmidt, and F. Mila, *Phys. Rev. Lett.* **111**, 137204 (2013).

- [10] S. Haravifard, D. Graf, A. E. Feiguin, C. D. Batista, J. C. Lang, D. M. Silevitch, G. Srajer, B. D. Gaulin, H. A. Dabkowska, and T. F. Rosenbaum, *Nat Commun* **7**, 11956 (2016).
- [11] T. Waki, K. Arai, M. Takigawa, Y. Saiga, Y. Uwatoko, H. Kageyama, and Y. Ueda, *Journal of the Physical Society of Japan* **76**, 073710 (2007), <https://doi.org/10.1143/JPSJ.76.073710>.
- [12] T. Sakurai, Y. Hirao, K. Hijii, S. Okubo, H. Ohta, Y. Uwatoko, K. Kudo, and Y. Koike, *Journal of the Physical Society of Japan* **87**, 033701 (2018), <https://doi.org/10.7566/JPSJ.87.033701>.
- [13] M. E. Zayed, C. Rüegg, J. Larrea J., A. M. Läuchli, C. Panagopoulos, S. S. Saxena, M. Ellerby, D. F. McMorrow, T. Strässle, S. Klotz, G. Hamel, R. A. Sadykov, V. Pomjakushin, M. Boehm, M. Jiménez-Ruiz, A. Schneidewind, E. Pomjakushina, M. Stingaciu, K. Conder, and H. M. Rønnow, *Nature Physics* **13**, 962 (2017).
- [14] B. S. Shastry and B. Sutherland, *Physica B+C* **108**, 1069 (1981).
- [15] S. Miyahara and K. Ueda, *J. Phys.: Condens. Matter* **15**, R327 (2003).
- [16] M. Albrecht and F. Mila, *Europhys. Lett.* **34**, 145 (1996).
- [17] S. Miyahara and K. Ueda, *Phys. Rev. Lett.* **82**, 3701 (1999).
- [18] Z. Weihong, C. J. Hamer, and J. Oitmaa, *Phys. Rev. B* **60**, 6608 (1999).
- [19] E. Müller-Hartmann, R. R. P. Singh, C. Knetter, and G. S. Uhrig, *Phys. Rev. Lett.* **84**, 1808 (2000).
- [20] A. Koga and N. Kawakami, *Phys. Rev. Lett.* **84**, 4461 (2000).
- [21] Y. Takushima, A. Koga, and N. Kawakami, *J. Phys. Soc. Jpn.* **70**, 1369 (2001).
- [22] C. H. Chung, J. B. Marston, and S. Sachdev, *Phys. Rev. B* **64**, 134407 (2001).
- [23] A. Läuchli, S. Wessel, and M. Sgrist, *Phys. Rev. B* **66**, 014401 (2002).
- [24] W. Zheng, J. Oitmaa, and C. J. Hamer, *Phys. Rev. B* **65**, 014408 (2001).
- [25] P. Corboz and F. Mila, *Phys. Rev. B* **87**, 115144 (2013).
- [26] M. Moliner, I. Rousochatzakis, and F. Mila, *Phys. Rev. B* **83**, 140414 (2011).
- [27] For details on the iPEPS, the SE, and the excitations of the two-dimensional distorted Shastry-Sutherland model, see Supplementary Material.
- [28] F. Verstraete and J. I. Cirac, *arXiv:cond-mat/0407066* (2004), [arXiv: cond-mat/0407066](https://arxiv.org/abs/cond-mat/0407066).
- [29] Y. Nishio, N. Maeshima, A. Gendiar, and T. Nishino, Preprint (2004), [arXiv:cond-mat/0401115](https://arxiv.org/abs/cond-mat/0401115).
- [30] J. Jordan, R. Orús, G. Vidal, F. Verstraete, and J. I. Cirac, *Phys. Rev. Lett.* **101**, 250602 (2008).
- [31] P. Corboz and F. Mila, *Phys. Rev. Lett.* **112**, 147203 (2014).
- [32] P. Corboz, R. Orús, B. Bauer, and G. Vidal, *Phys. Rev. B* **81**, 165104 (2010).
- [33] H. N. Phien, J. A. Bengua, H. D. Tuan, P. Corboz, and R. Orús, *Phys. Rev. B* **92**, 035142 (2015).
- [34] P. Löwdin, *The Journal of Chemical Physics* **19**, 1396 (1951), <https://doi.org/10.1063/1.1748067>.
- [35] P. Löwdin, *Journal of Mathematical Physics* **3**, 969 (1962), <https://doi.org/10.1063/1.1724312>.
- [36] T. Kato, *Phys. Rev.* **77**, 413 (1950).
- [37] C. Knetter and G. S. Uhrig, *Eur. Phys. J. B* **13**, 209 (2000).
- [38] C. Knetter, K. P. Schmidt, and G. S. Uhrig, *Journal of Physics A: Mathematical and General* **36**, 7889 (2003).
- [39] Y. Takushima, A. Koga, and N. Kawakami, *Journal of the Physical Society of Japan* **70**, 1369 (2001), <https://doi.org/10.1143/JPSJ.70.1369>.
- [40] M. Arlego and W. Brenig, *Phys. Rev. B* **78**, 224415 (2008).
- [41] M. Arlego and W. Brenig, *Phys. Rev. B* **84**, 134426 (2011).
- [42] A. C. Guttman, *Phase Transitions and Critical Phenomena*, edited by C. Domb and J. Lebowitz, Vol. 13 (Academic Press, New York, 1989).
- [43] A. Honecker, S. Wessel, R. Kerkdyk, T. Pruschke, F. Mila, and B. Normand, *Phys. Rev. B* **93**, 054408 (2016).
- [44] P. Corboz and F. Mila, *Phys. Rev. B* **87**, 115144 (2013).
- [45] S. Singh, R. N. C. Pfeifer, and G. Vidal, *Phys. Rev. B* **83**, 115125 (2011).
- [46] B. Bauer, P. Corboz, R. Orús, and M. Troyer, *Phys. Rev. B* **83**, 125106 (2011).
- [47] H. C. Jiang, Z. Y. Weng, and T. Xiang, *Phys. Rev. Lett.* **101**, 090603 (2008).
- [48] P. Corboz, *Phys. Rev. B* **94**, 035133 (2016).
- [49] T. Nishino and K. Okunishi, *J. Phys. Soc. Jpn.* **65**, 891 (1996).
- [50] R. Orús and G. Vidal, *Phys. Rev. B* **80**, 094403 (2009).
- [51] P. Corboz, S. R. White, G. Vidal, and M. Troyer, *Phys. Rev. B* **84**, 041108 (2011).
- [52] P. Corboz, T. M. Rice, and M. Troyer, *Phys. Rev. Lett.* **113**, 046402 (2014).
- [53] P. Corboz, *Phys. Rev. B* **93**, 045116 (2016).
- [54] T. Nishino and K. Okunishi, *J. Phys. Soc. Jpn.* **65**, 891 (1996).
- [55] H.-Y. Yang, A. M. Läuchli, F. Mila, and K. P. Schmidt, *Phys. Rev. Lett.* **105**, 267204 (2010).
- [56] J. Röchner, L. Balents, and K. P. Schmidt, *Phys. Rev. B* **94**, 201111 (2016).
- [57] K. Coester and K. P. Schmidt, *Phys. Rev. E* **92**, 022118 (2015).
- [58] K. P. Schmidt and G. S. Uhrig, *Phys. Rev. Lett.* **90**, 227204 (2003).
- [59] N. Ivanov and J. Richter, *Physics Letters A* **232**, 308 (1997).
- [60] S. R. White and D. A. Huse, *Phys. Rev. B* **48**, 3844 (1993).
- [61] O. Golinelli, T. Jolicoeur, and R. Lacaze, *Phys. Rev. B* **50**, 3037 (1994).
- [62] J. Richter, N. B. Ivanov, and J. Schulenburg, *Journal of Physics: Condensed Matter* **10**, 3635 (1998).
- [63] A. Koga, K. Okunishi, and N. Kawakami, *Phys. Rev. B* **62**, 5558 (2000).